Cell Reports
Physical Science

CellPress
OPEN ACCESS

Article

A non-volatile thermal switch for building energy savings

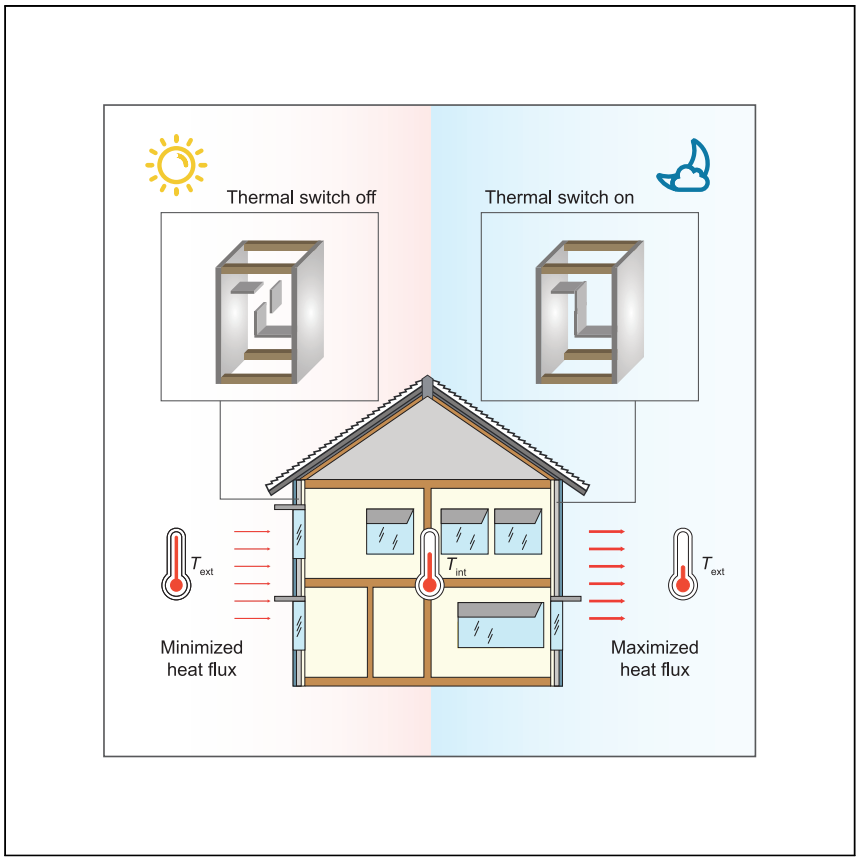

Like opening and closing windows, a thermally switchable building envelope could reduce heating and cooling loads by selectively coupling/decoupling to the exterior environment when beneficial. Miao et al. experimentally demonstrate a voltage-driven thermal switch suitable for this application. The bi-stable mechanism minimizes the energy required for device operation.

Ruijiao Miao, Ravi Kishore, Sumanjeet Kaur, Ravi Prasher, Chris Dames

rsprasher@lbl.gov (R.P.)
cdames@berkeley.edu (C.D.)

Highlights

Bi-stable voltage-controlled thermal switch designed for building envelopes

Low off-state thermal conductivity of 0.045 W $m^{-1}K^{-1}$ is close to fiberglass

Simulations show 9%–55% and 17%–76% annual energy savings for heating and cooling

Miao et al., Cell Reports Physical Science 3, 100960
July 20, 2022
https://doi.org/10.1016/j.xcrp.2022.100960

Cell Reports
Physical Science

CellPress
OPEN ACCESS

Article

A non-volatile thermal switch for building energy savings

Ruijiao Miao,[1,2] Ravi Kishore,[3] Sumanjeet Kaur,[1] Ravi Prasher,[1,2,*] and Chris Dames[1,2,4,*]

SUMMARY

Compared with traditional static insulation, a thermally switchable building envelope could reduce annual heating and cooling loads by intermittently coupling to the outside environment when beneficial. Here, we demonstrate a voltage-actuated, contact/non-contact thermal switch that meets the unique challenges of this application. The switch is non-volatile, consuming electricity only briefly while switching and none to hold steady state. The switch ratio is 12, the off state has a low effective thermal conductivity of 0.045 W $m^{-1}K^{-1}$, comparable to fiberglass insulation, and the performance is stable over 1,000 switching cycles. Numerical simulations using real-world climate data show that combining this thermal switch with a thermal storage layer in a building envelope can yield annual energy savings of 9%–55% (heating) and 17%–76% (air conditioning), depending on the climate zone. The greatest benefits are realized when the exterior temperature crosses well above and below the desired interior temperature within a single 24 h period.

INTRODUCTION

The energy used for space heating and cooling in buildings (heating, ventilation, and air conditioning [HVAC]) is a major part of worldwide energy consumption[1] and is one of the top challenges for the building industry.[2,3] In the United States, for example, residential and commercial building energy use accounts for 28% of the total end-use energy and 40% of the total energy consumption when electrical system losses are considered.[4] Similarly, space heating makes up 43% of total residential energy end use.[5] It also is important to reduce the thermal load in buildings because air conditioning and heat pumps use refrigerants of high global warming potential.[6]

Building envelopes lose energy through their windows, roof, and walls (Figure 1A). For windows, next-generation electrochromics or thermochromics have switchable optical properties that can be modulated based on climate conditions.[7–9] Similarly, for roofs, switchable radiative materials have been developed and demonstrated that can change properties depending on temperature.[10–12] In contrast, the thermal-insulation performance of the opaque envelope walls (typically having the largest area among all envelope components[13]) is generally seen as static, not switchable. This is an important opportunity, since modeling has shown that envelopes with a switchable thermal conductance in response to changing temperature (both diurnal and seasonal) can yield major reductions in building thermal loads[14–19] (a simplified scenario is shown in Figures 1B and 1C, with detailed energy savings presented in Figure 6 for simulations of realistic envelopes and climates). The principal benefits are realized when the exterior temperatures cross significantly both

[1]Lawrence Berkeley National Laboratory, Berkeley, CA 94720, USA

[2]Department of Mechanical Engineering, University of California, Berkeley, Berkeley, CA 94720, USA

[3]National Renewable Energy Laboratory, Golden, CO 80401, USA

[4]Lead contact

*Correspondence: rsprasher@lbl.gov (R.P.), cdames@berkeley.edu (C.D.)

https://doi.org/10.1016/j.xcrp.2022.100960

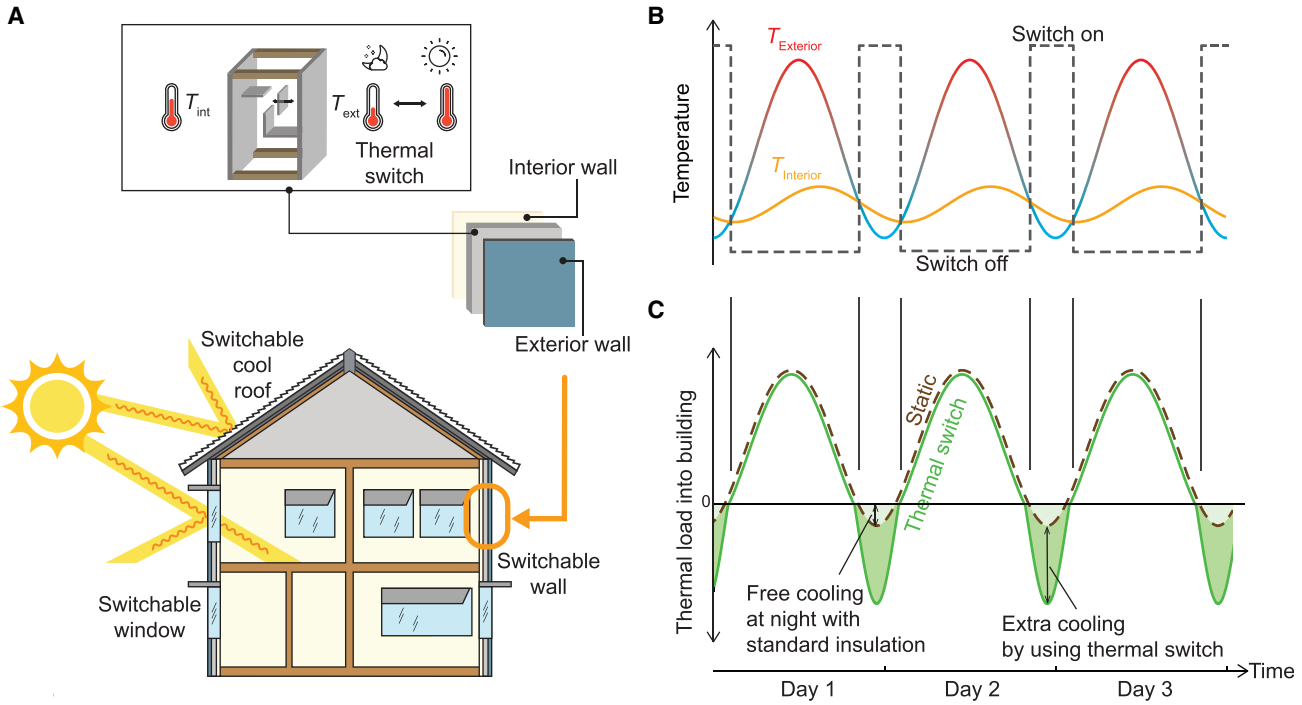

Figure 1. Concept of a thermal switch for building-envelope thermal management

(A) Schematic of a variable environmental T_{ext} linked to the building interior T_{int} through three thermal pathways (roof, windows, walls). Zoom-in schematics show the wall with thermal switches (i.e., functioning as dynamic insulation) located inside the wall cavity. The thermal switches can be opened or closed on demand to either isolate or couple the interior and exterior environments to minimize HVAC demand while maintaining a comfortable T_{int}.

(B) Representative exterior environment temperature (red/blue line), desired interior temperature (orange line), and state of thermal switch (gray dashed line), all versus time over 3 days. In this simplified but representative summertime scenario, the switch toggles into the on (high-*k*) state in the late-night hours to take advantage of free cooling from the environment.

(C) Corresponding thermal load through the wall into the building versus time, without (brown dashed line) and with (green solid line) thermal switches. Negative values of the thermal load are desirable here, as they indicate free cooling at night by the exterior environment. This nighttime cooling is increased by using thermal switches (darker green shaded area). Note the curves in (B) and (C) are simplified schematics to explain the concept. Detailed numerical simulations for a realistic wall with embedded switches are presented later in Figures 5 and 6.

above and below the desired interior temperature within a 24 h period. Indeed, the need to develop variable-conductance building envelopes was recently highlighted as a thermal-energy grand challenge for decarbonization.[20] However, the experimental demonstration of a thermal switch suitable for this envelope application remains lacking.

A switchable building envelope, with static insulation replaced by an active thermal switch functionality,[21] can save energy by offering a "best of both worlds" solution. (1) Like traditional insulation, the "off" state of the switch minimizes undesired thermal loads from the environment to the interior. (2) For those times when the exterior conditions are favorable, the insulation switches to its thermally conducting "on" state to take advantage of the environment. A familiar example is a clear sunny day in late summer (Figures 1B and 1C). During the hot daytime hours, the wall should be insulating to minimize heat uptake from the environment and lessen the need for air conditioning. Then, late at night, the wall should switch to a thermally conducting state to take advantage of the free cooling from the colder nighttime environment. While these two switch regimes are analogous to opening and closing windows, switching the opaque envelope offers several advantages in principle, such as covering a larger total wall area, suitability for automation (as long as the

thermal switch is controlled electrically, as in the present work), and being much less disruptive from the perspectives of outside sound, wind, and security.

The potential energy savings from a switchable thermal envelope are expected to be substantial based on prior modeling studies.[14,15,19,22–26] For example, Menyhart and Krarti[14] analyzed a variety of idealized thermal switches for 15 climate zones across the United States and found heating and cooling energy savings ranging from 7% to 42% compared with traditional static insulation. As another important benefit, switchable building envelopes enable time shifting the HVAC demand. This peak-shifting and -shaving capability is expected to become even more important as renewable energy sources further permeate the grid.[27–29]

To date, these potential benefits of switchable building envelopes have been based on modeling rather than experiments.[14,15,19,22–25] Developing a working thermal switch for this building-envelope application introduces several unique challenges compared with prior switches.[21] Most fundamentally, this application calls for a very low effective thermal conductivity in the off state, $k_{eff,off}$, which should be close to that of existing static insulation like fiberglass, as well as a high switching ratio, $r \geq 10$, guided by previous modeling[19,30] While such r values have been widely reported,[21] to the best of our knowledge, such a low $k_{eff,off}$ is unprecedented and has not been of interest in prior switch demonstrations, which generally involve $k_{eff,off}$ values at least an order of magnitude larger than what is demonstrated here. Another key challenge is to greatly minimize the energy required for switching. Additional criteria include cyclability, cost, and fixed package size.[19] As surveyed recently by Cui and Overend,[31] a variety of existing thermal switch technologies that were developed for other applications could also be considered for the building-envelope application, such as variable conductance heat pipes, vacuum gas-gap thermal switches, magnetically aligned nanofluids, and switched-pump convection (also like Ciampi et al.[32]), though close consideration indicates that none of those pre-existing switch technologies can meet all the challenges described above.

Here, we design and demonstrate a voltage-actuated, contact/non-contact thermal switch specifically to meet these challenging criteria. Related contact-based thermal control, including shape memory alloy (SMA) and wax-based actuators, has been developed for thermal diodes and regulators,[31,33–37] with applications including thermal management of batteries and spacecraft.[36–39] In contrast to those passive, two-terminal devices, the present work differs fundamentally in that a thermal switch is active and has a 3rd terminal, which is used for on-demand control via the applied voltage. Furthermore, we incorporate a non-volatile mechanism[40] that consumes electricity only briefly while switching a bi-stable thermal contact and none to maintain steady state. This greatly reduces the total electrical energy consumption of the switch by more than three orders of magnitude compared with alternative switching schemesthat would require continuous electricity to hold the switch in one of its two states.

As demonstrated below, this switch has a very low off-state thermal conductivity ($k_{eff,off}$ = 0.045 W $m^{-1}K^{-1}$, which is similar to traditional building-insulation material), high switch ratio (r = 12.2), good cyclability (1,000 cycles demonstrated), thin package size (5 cm), and low switching energy (1,000–4,600 J/m^2 per change of state), all of which are promising for the building-envelope application. Finally, numerical simulations of realistic building envelopes and climate-zone data highlight the potential for 9%–55% reductions in heat loss and 17%–76% reductions in heat gains, depending on the season and climate zone.

RESULTS AND DISCUSSION

Thermal switch design and working principle

A thermal switch uses a non-thermal control parameter to toggle its thermal conductance, G, between maximum and minimum values, G_{on} and G_{off}, respectively.[21] After normalizing by the external dimensions of the device (cross-sectional area $A = W^2$, thickness H; see Figure 2A), the corresponding effective thermal conductivities are $k_{eff,on} = \frac{G_{on}H}{A}$ and $k_{eff,off} = \frac{G_{off}H}{A}$, and the switch ratio is

$$r = k_{eff,on}/k_{eff,off}. \quad \text{(Equation 1)}$$

Here, we design a thermal switch based on connecting/breaking a thermal pathway, as shown in Figures 2A and 2B. The switch has a fixed exterior geometry (W = 10 cm, H = 5 cm), which is representative of a unit cell element that could be scaled up and/or tiled for application inside a building envelope; for example, typical wall cavities in the United States are 3.5″ to 5.5″ (= 9–14 cm) thick (an example of this tiling concept is given later in Figure 5). For the present demonstration, aluminum is employed as the heat-conduction medium due to its high thermal conductivity, light weight, and reasonable cost, and high-density polyethylene (HDPE) plastic with low thermal conductivity is used to define the four corners of the device frame. As shown in Figure 2A, the gap between the moving bridge plate and the two stationary face plates defines the on (gap closed, $d = 0$) and off (gap open, $d > 0$) states of the switch.

Joule-heated SMA wires are used to activate the opening and closing of this gap; recall that related SMA-based devices were passive thermal diodes and regulators[33–35] without any voltage control, while the present work is an active thermal switch. The SMA effect is well understood and widely used in medical and some automotive applications.[41] The key here is that an SMA wire undergoes a reversible martensitic transformation around its nominal phase transition temperature T_{trans} (chosen here to be 70°C, i.e., well above the highest anticipated environmental temperature in order to avoid unintended switching). When heated to $T_{high} > T_{trans}$, the SMA wire shrinks in length with a strain $\Delta\varepsilon$ between 2% to 8% at constant stress ($\Delta\varepsilon$ = 3% for the chosen SMA wire).[41,42] When temperature decreases to $T_{low} < T_{trans}$, the deformation can be easily reversed by a modest external pulling force.

The switching mechanism is as follows. As illustrated in Figure 2C, an antagonistic pair of SMA wires are mounted along the frame top plate, with their ends connected to the outer (SMA1) or inner (SMA2) ends of the two pivot blocks. These rotating blocks also clamp onto the ends of a steel spring beam. Switching the device to its on state is initiated by applying a voltage (typically 3–4 V) to the outer SMA wire (SMA1). The resulting joule heating brings the wire T above T_{trans}, causing it to contract by an estimated s_{max} = 4.4 mm (see Note S1 and Figure S1 for details). This pulls the outermost ends of the two pivot blocks upwards, causing the spring beam to snap downwards, which pushes the bridge plate into contact with the face-plate regions of the aluminum frame. This places the device in the on state, with the heat-flow path indicated in Figure 2B (top). Thin sheets of thermal interface material (TIM) are used to improve the thermal contact. After this switching operation, the voltage applied to SMA1 is removed, and it cools freely to room temperature. Crucially, due to the bi-stable snap-through mechanism of the spring beam,[40] the device now maintains its on state indefinitely, without any further electricity consumption.

Similarly, to switch to the off state, the inner SMA wire (SMA2 in Figure 2C) is joule heated. Since SMA1 is in its relaxed state, the contracting force of SMA2 is enough

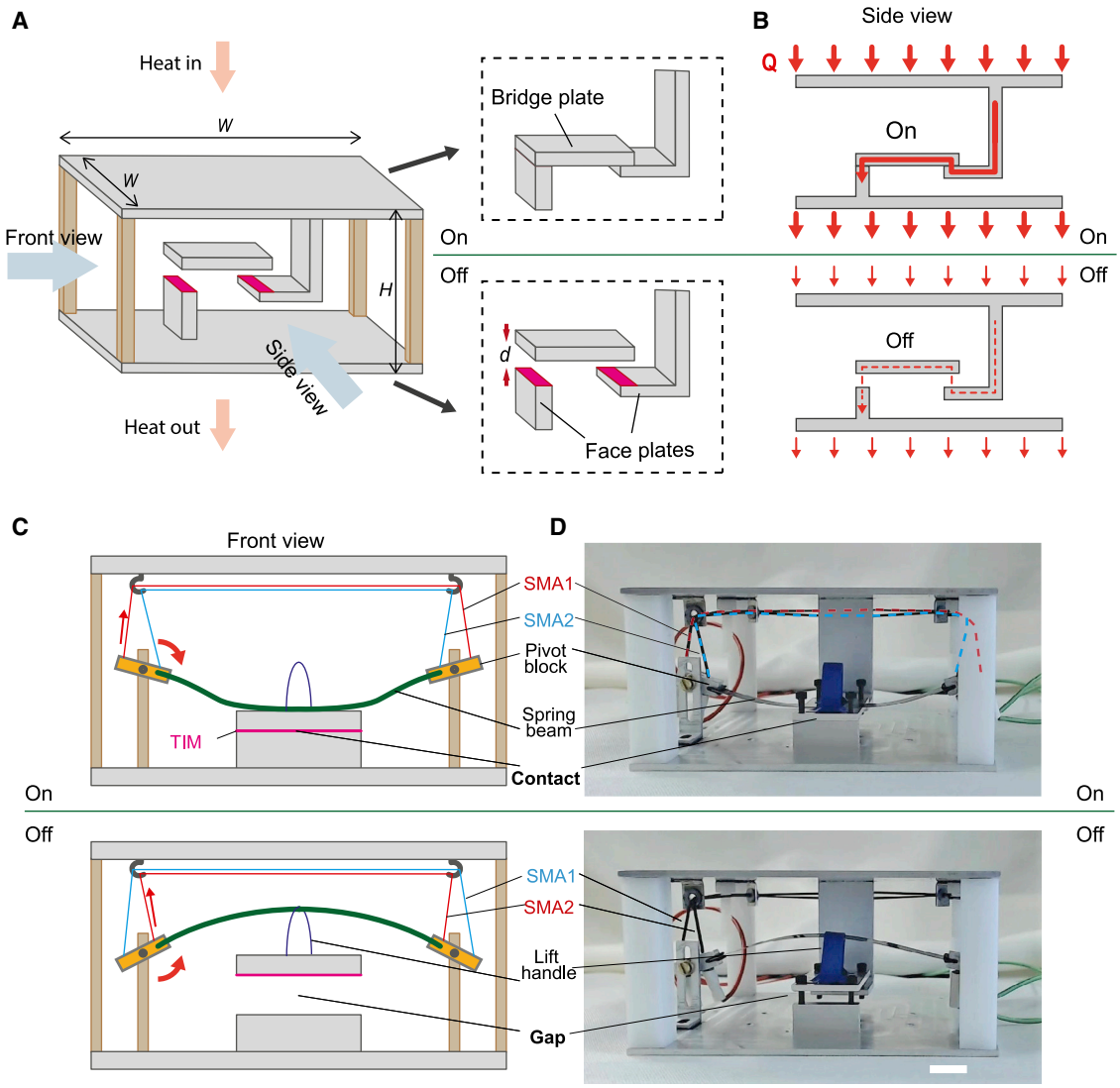

Figure 2. Voltage-controlled bi-stable thermal switch

(A) Schematics showing the device structure and thermal switching principle: for the on state, the bridge plate contacts the two TIM rectangles to form a heat-conducting pathway, while in the off state they are separated by a gap *d*. Here, the silver components are aluminum, brown are HDPE plastic, and pink are TIM.

(B) Primary thermal path for on (top schematic) and off (bottom schematic) states.

(C and D) Schematics and photos showing the bi-stable switching mechanism between on (top schematic) and off (bottom) states. The ends of the SMA wires are connected to an external voltage source for active control (not shown in C). When either SMA wire is joule heated (red color), it contracts and rotates the ends of the pivot blocks, which causes the spring beam to snap down (when SMA1 is heated) or up (SMA2 heated) between its two stable states. When the SMA wires are both de-energized, they are both slack, and the spring beam maintains its last state without any electricity consumption, a fundamental distinction from previous related works.[33–35] In (C), the central vertical post of the aluminum frame has been omitted to simplify the schematic. In (D), the brightness and contrast have been adjusted for clarity, and the scale bar is approximately 1 cm (i.e., $W = 10$ cm and $H = 5$ cm). In the top panel of (D), dashed colored lines have been overlaid on the SMA wires for ease of identification.

to rotate the pivot blocks again, now snapping the spring beam upwards and lifting the moving plate through a thin plastic "lift handle." This creates the air gap *d* between the bridge plate and face plates, which breaks the thermal path (Figure 2B, bottom) and minimizes the heat flow. The rotating of the pivot blocks also pulls SMA1 back to its original length. And again, this device state is maintained indefinitely even after the voltage is removed from SMA2.

A key feature of this scheme is that the thermal switch is non-volatile and stable in both its on and off states. No electricity is required to hold either steady state. This is essential for lowering the overall energy consumption of this thermal switch for the building-envelope application, which should only require switching one or two times per day. As each switching operation lasts less than 10 s (see Note S6), this means that the thermal switch would consume electricity only ~0.01% of any given day and would passively hold its state the other 99.99% of the time. In contrast, a simpler thermal switch (such as plausible extensions of the previous diodes or regulators[33–35]) would have to apply joule heating continuously to hold one of the two states, thereby consuming electricity for ~50% of the year on average (i.e., over three orders of magnitude greater energy consumption than the non-volatile approach).

Having established the basic operating mechanism depicted in Figures 2A–2C, we then proceeded to design a thermal switch device for this building application. Based on previous modeling,[14,19] we targeted low $k_{eff,off} \leq 0.05$ W m^{-1}K^{-1} and high $r \sim 5$–10. For a variety of geometries and dimensions, we used a numerical finite element model (COMSOL software) to simulate the heat flow in each state (see Note S2). The chosen design is shown in Figure 2D. For this design, the predicted performance (see Figure S2) is $k_{eff,on} = 0.56$ W m^{-1}K^{-1}, $k_{eff,off} = 0.040$ W m^{-1}K^{-1}, and $r = 14$, which satisfies the key performance targets.

Effective thermal conductivity and switch ratio test

To quantify the performance of this thermal switch device experimentally, we define the effective thermal conductivity by treating the device as a lumped "black box," so that

$$k_{eff,on/off} = \frac{Q_{on/off} H}{A(T_{hot} - T_{cold})}. \quad \text{(Equation 2)}$$

Here, Q is the heat flow through the device, and this definition applies to both on and off states, as indicated by the dual subscripts.

Figure 3A shows an experimental setup to test the performance of the thermal switch device. A film heater was attached to the top of the device to provide heating power Q, and the bottom of the device was connected to an air-cooled heat sink (see experimental procedures). The sides of the device and top of the film heater were thermally insulated. Thermocouples were mounted with silicone grease to the top and bottom of the device to monitor T_{hot} and T_{cold}. Prior to each measurement, the device was switched to the designated state (on or off) by applying a voltage to the appropriate SMA wire for 20 s and then removing the voltage, and then the entire device was allowed to come to equilibrium with the surrounding ambient temperature.

To measure $k_{eff,off}$, at time $t = 0$ the film heater was set to dissipate $Q_{off} = 0.22$ W. This is a relatively low heat rate, chosen to ensure that both T_{hot} and T_{cold} remained well below the SMA transition temperature ($T_{trans} = 70°C$) so as to avoid accidentally activating an SMA wire. After T_{hot} and T_{cold} reached steady state, they were recorded and used to calculate $k_{eff,off}$ from Equation (2). An example of this $k_{eff,off}$ measurement is shown in Figure 3B. At steady state, the measured $\Delta T = T_{hot} - T_{cold} = 24.9°C$, yielding $k_{eff,off} = 0.043$ W m^{-1}K^{-1}.

The same procedure was subsequently used to measure $k_{eff,on}$ (Figure 3C). The result is $k_{eff,on} = 0.63$ W m^{-1}K^{-1} and thus a switch ratio of $r = 14.6$. The linearity of the thermal

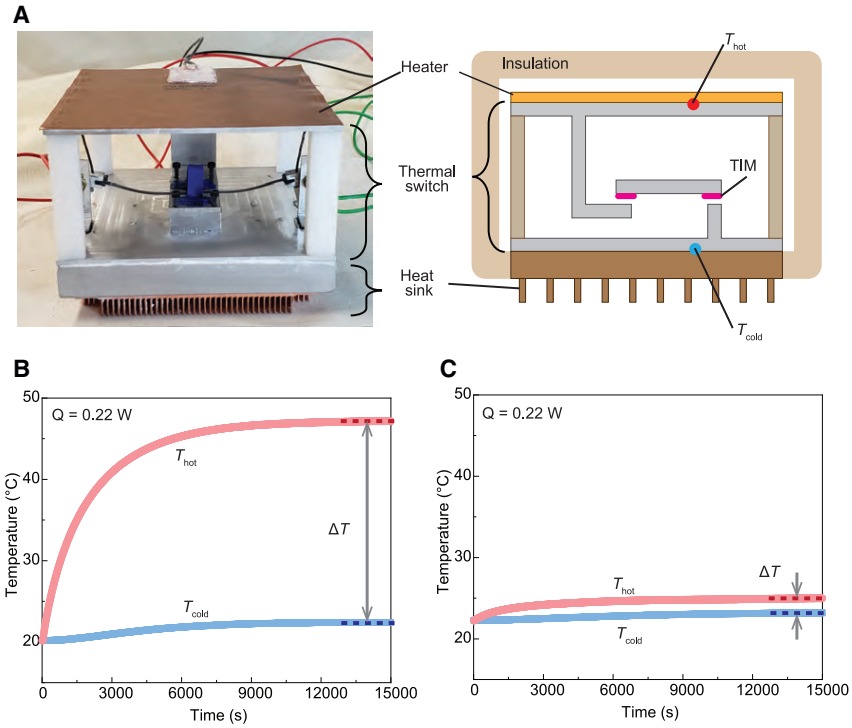

Figure 3. Thermal switch device performance test

(A) Photo (front view, with insulation removed) and schematic (simplified side view) of setup for measuring the effective thermal conductivity.

(B and C) Measurements of temperature versus time for off (B) and on (C) states, each in response to a step change in heater power from Q = 0 to 0.22 W at time t = 0. Using Equation (2), the corresponding effective thermal conductivities are $k_{eff,off}$ = 0.043 W $m^{-1}K^{-1}$ and $k_{eff,on}$ = 0.63 W $m^{-1}K^{-1}$, giving a switch ratio r = 14.6.

response (ΔT versus Q) in both on and off states is verified experimentally in Note S3 and Figure S3. We note that the measured $k_{eff,off}$ and $k_{eff,on}$ values are in reasonable agreement with the numerical predictions of the COMSOL model, thereby helping confirm the suitability of the model as well. These results indicate that this type of device can meet the key heat-transfer criteria needed for the building-envelope application.[14,19]

Cyclability test

For building applications, this thermal switch device will also need high cyclability. Thus, to evaluate the repeatability of the gap size and effective thermal conductivity, we performed two different tests, each of 1,000 on/off cycles. The first test was to investigate the cyclability of the gap size, by recording a video of 1,000 continuous on/off cycles using a digital camera. The film heater and insulation materials were removed for this test because they were unnecessary. Each on/off cycle has four phases: (1) the wire SMA1 was joule heated for 20 s to close the gap (during this time, no voltage was applied to SMA2); (2) all SMA voltages were off for 40 s, allowing SMA1 to cool freely back to room temperature while the gap stayed closed; (3) then, similarly, SMA2 was Joule heated for 20 s to open the gap; and finally, (4) all SMA voltages were off for 40 s, allowing SMA2 to cool freely back to room temperature while the gap stayed open. The entire 1,000 cycle video is available as Video S1, which qualitatively confirms the repeatability of this gap opening and closing. Furthermore, to more quantitatively analyze this process, every 50 cycles the

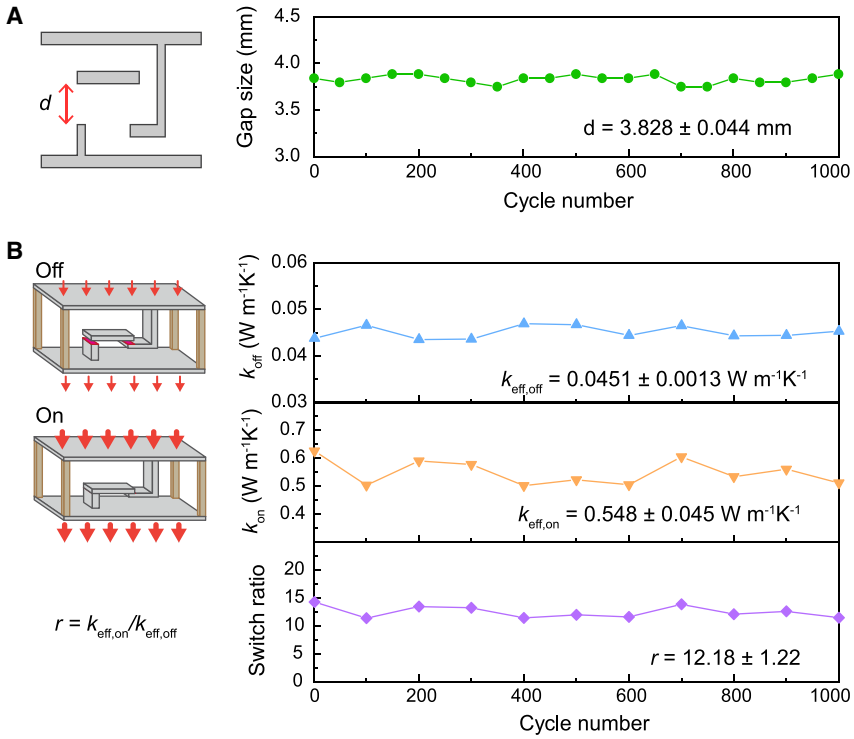

Figure 4. Cyclability tests

(A) Off-state gap size for 1,000 switch cycles, measured every n = 50 cycles. A continuous movie with all 1,000 cycles is given as Video S1.

(B) On- and off-state thermal conductivity and switch ratio during another 1,000 switch cycles, measured every n = 100 cycles. Top and bottom schematics correspond to off- and on-state thermal conductivity measurements, respectively.

off-state gap size was evaluated directly from the video images using a separate calibration that each camera pixel corresponds to 30 μm at the image plane. The results of this gap cycling test are given in Figure 4A, which shows that the off-state gap size was consistent over 1,000 cycles as 3.828 ± 0.044 mm (mean ± SD).

These optical measurements of repeatable air gap d in the off state indicate repeatable off-state performance over 1,000 cycles. For the on state, however, this imaging approach cannot measure the compression of the TIM or the contact pressure when the gap is fully closed, which are important factors for $k_{eff,on}$. Therefore, to evaluate the cyclability directly in terms of thermal performance, we repeated the 1,000 cycle test (SMA voltages cycling through the same 4 phases as described in the previous paragraph) with a fully thermally insulated device, except this time, we also paused the testing every 100 cycles to measure the on- and off-state thermal conductivities in the same way as Figure 3. Figure 4B (see also Table S1) gives the resulting values for $k_{eff,off}$, $k_{eff,on}$, and r, which exhibit stable thermal performance over the 1,000 cycles, with relatively tight SDs of ±2.9%, 8.2%, and 10% of their respective means. Note the $k_{eff,off}$ = 0.0451 W m^{-1}K^{-1} is close to fiberglass insulation (0.032–0.049 W m^{-1}K^{-1} at 25°C).[43,44] Representative raw thermal test data for cycles 1, 500, and 1,000 are also presented in Note S4 and Figure S4.

Finally, we also confirmed that the device functions well regardless of orientation, which is also important for applications in a building envelope. Videos S2 and S3 show 10 consecutive switching cycles with the switch sideways and upside down,

respectively, which confirm that the bi-stable mechanism depicted in Figure 2 continues to operate regardless of orientation. Note S5 presents heat-transfer measurements similar to Figure 3, except that the heater is at the bottom and the cooling is at the top, which is expected to enhance natural convection if it plays a significant role. As shown in Figure S5, this measurement gives $k_{eff,off}$ = 0.044 W $m^{-1}K^{-1}$ and $k_{eff,on}$ = 0.61 W $m^{-1}K^{-1}$. These reversed-direction measurements are within 2% and 11%, respectively, of the results from Figure 4 for the original orientation, confirming that natural convection does not play an important role and that the thermal performance of the switch is largely independent of orientation.

Estimating material and energy costs for a building-integrated thermal switch

For potential building applications, the material cost and energy consumption to operate the thermal switch device are important considerations. We start with the energy consumption. To quantify the required switching time and energy for the present device, we conducted transient switching experiments using various SMA heating voltages. As detailed in Note S6 and summarized in Table S2, after optimizing the applied voltage, the time to switch the device from closed to open can be less than 1 s, consuming less than 5 J of electrical energy per switching event. Closing the device is slower (best case time was between 5 and 6 s) and consumes more energy (~23 J per switching event). This discrepancy between opening and closing is not a fundamental limitation but rather arises from the different shape of the spring beam in the two states, as explained in Note S6.

To scale this electricity consumption to an entire house, we assume a representative residential house exterior wall area of ~150 m^2[13,45] and a double layer of thermal switches, each undergoing one on-off-on cycle daily. With the optimized switching voltages and durations, the estimated monthly energy cost in electricity to operate these thermal switches for the entire house is 6.7 kWh_e/house/month. Assuming half of this joule heat returns to the interior of the house, on a wall-area-normalized basis the corresponding thermal load back into the house is 22 Wh_{th}/m^2/month, which burdens the air conditioning in the summer months while being advantageous in winter months. The units of Wh_{th}/m^2/month are chosen to facilitate comparison with the model calculations below in Figure 6B. As discussed further below, these calculations show that the typical air conditioning energy savings from using these thermal switches in the summer months are several 100s of Wh_{th}/m^2/month, which more than compensates for this 22 Wh_{th}/m^2/month parasitic burden from the switching energy.

Turning now to the materials cost, as an initial feasibility check we made estimates based on bulk (tonne-scale) pricing of the major constituent materials[46] and the geometry of the test device depicted in Figure 2. Details are given in Table S3. Briefly, the SMA wires are made from 45% Ti and 55% Ni (wt %), which are relatively expensive metals, but the amount used in the thermal switch device is very small due to the thin wire diameter (250 μm), so that the SMA wires make up less than 0.2% of the device mass and 1.3% of its estimated cost. In this design it is the aluminum, as the frame material, that dominates both the weight (92%) and estimated cost (84%). For an H = 5 cm thick thermal switch device, as shown in Figure 2, the total material cost including SMA, aluminum, HDPE, and TIM is estimated to be \$14.6/m^2 as normalized by the device area ($W \times W$). For comparison, the cost of traditional static fiberglass insulation is ~4–6 \$/kg, corresponding to 3–5 \$/m^2 with the same thickness. Accounting for a double layer of thermal switches scaled to tile an entire house with ~150 m^2 wall area (see Note S7), the total raw material cost is estimated as \$4,400 per house.

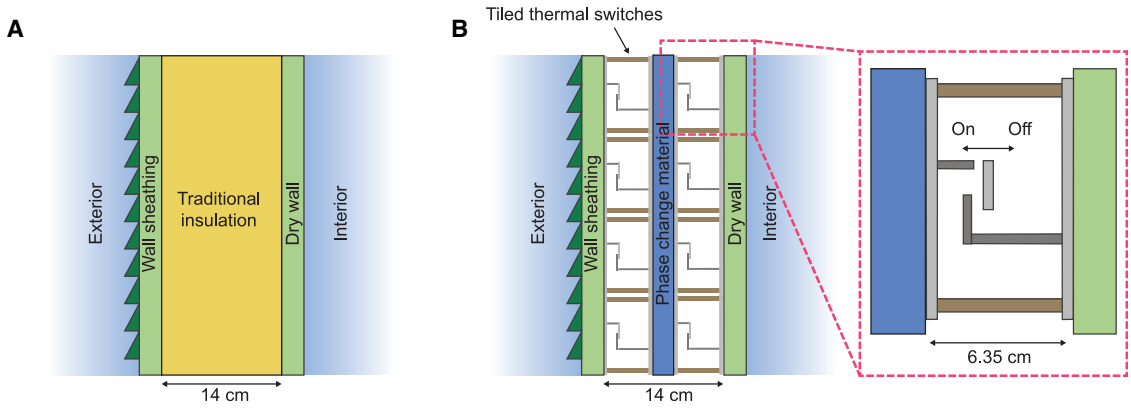

Figure 5. Concept of thermal switch devices integrated within a building envelope

(A) Traditional wall cavity with fiberglass insulation. For clarity, the wooden studs are not shown.

(B) This work: example of tiling of thermal switch devices within a wall cavity. The wooden studs (not shown) are also still present. The inset shows a detailed view of a single switch device as a tiling unit. Two layers of thermal switches are tiled and sandwich a PCM layer inside a building wall. For the simulations presented in Figure 6, the wall cavity (switches + PCM) is 14 cm (5.5″), composed of a 1.27 cm (0.5″) thick layer of PCM, and thus $H = 6.35$ cm (2.5″) for each switch layer.

Modeled energy savings considering local climate zones

Now we discuss the potential energy savings in buildings equipped with this thermal switch device considering local climate types. While a single layer of wall-integrated thermal switches is effective in enhancing the utilization of ambient cooling/heating such as the scheme depicted in Figures 1B and 1C, our prior analysis[19] showed that further benefits are realized through incorporating a layer of phase change material (PCM) in the middle of the wall cavity sandwiched between two thermal switches, as depicted in Figure 5. The switch-PCM-switch stack replaces the traditional insulation, and the wood-stud structure is kept (see also Note S8). This configuration provides more flexibility and control to maximize the utilization of free ambient cooling/heating to charge the PCM and later discharge it toward the interior, thereby further reducing the thermal loads into the buildings. Note that the incorporation of PCM layers inside wall envelopes, without switchable insulation, is also an active area of research[47] that has already been tested in the field.

We quantify the energy savings for the wall structure depicted in Figure 5B (see also Figure S6). This switch-PCM-switch sandwich replaces the conventional static insulation. Figure 6A illustrates the operation of thermal switches for a few days in the cooling season for a climate like Baltimore (MD, USA) using standardized climate data[30,48] with 1 h step length. Here, we use a simple switching algorithm, which we have found to be effective, though it has no guarantee of being optimal (i.e., it may be possible to save more energy by further refining the algorithm). For the cooling season, the algorithm sets each switch to its off state whenever the temperature of the exterior side of that switch is higher than the interior side of the switch, thereby minimizing the heat in-flow directed toward the building interior. However, whenever the temperature of a thermal switch is lower toward its exterior side, it switches to the on state to take advantage of the free cooling. This scheme enables the free ambient cooling during the cool nighttime hours to solidify the PCM, which later liquifies during the hotter daytime hours, thereby dramatically reducing the heat gains through the building wall to the interior. This savings is quantified by comparing the orange and blue bars in the monthly total data shown in Figure 6B (top).

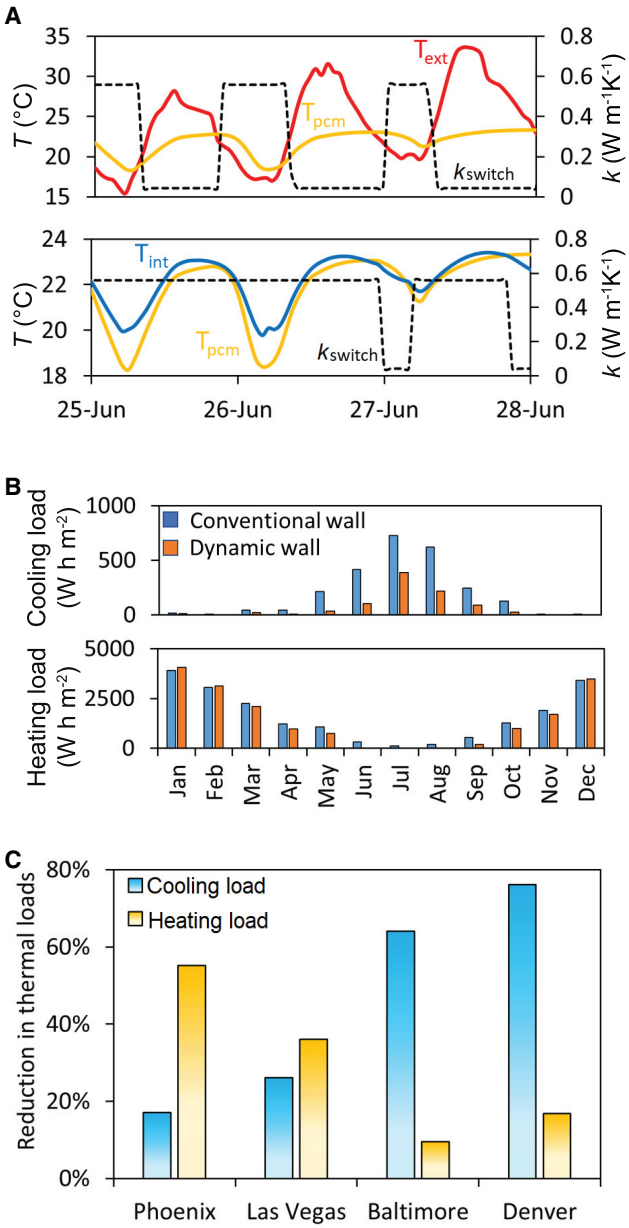

Figure 6. Simulation of energy savings in realistic climate zones

The chosen configuration of thermal switches sandwiching a PCM layer inside a building wall is depicted in Figure 5.

(A) Simulated operation of thermal switches over 3 representative days during the cooling season in Baltimore (MD, USA). The operation of the outer (inner) switch is depicted in the top (bottom) panel.

(B) Comparison between wall-related cooling (top) and heating (bottom) loads for walls with conventional static insulation (blue bars) and the dynamic wall configuration (orange bars), corresponding to Figures 5A and 5B, respectively. These calculations are for a standardized climate representative of Baltimore (MD, USA).

(C) The full-year energy savings for wall-related thermal loads, if using the configuration of Figure 5B versus conventional static insulation as in Figure 5A.

Although not depicted in Figure 6, the switching algorithm in the heating season is just the opposite: a thermal switch is set to be insulating when its exterior side is colder than its interior side and conducting when its exterior is hotter than its interior. This allows the free ambient heating to melt the PCM during the warm afternoon hours, while the PCM freezes during the cold nighttime hours, thereby reducing the heat losses from the interior through the building wall.

We have performed detailed calculations like Figure 6A for standardized climates[30,48] corresponding to four cities in the United States using switch performance metrics guided by the measurements in Figures 3 and 4, namely $k_{eff,on}$ = 0.559 W $m^{-1}K^{-1}$ and $k_{eff,off}$ = 0.043 W $m^{-1}K^{-1}$. See Note S8 and Table S4 for details. Representative results on a monthly basis are given in Figure 6B for Baltimore, and the total annual results for all four cities in Figure 6C. The combination of thermal switches and PCM reduces the wall-related heat gains by 17%, 26%, 64%, and 76% and the wall-related heat losses by 55%, 36%, 10%, and 17% in Phoenix (AZ, USA), Las Vegas (NV, USA), Baltimore, and Denver (CO, USA), respectively. Note that in the cooling season, the impact of thermal switches is greater when the summers are not too hot (e.g., Denver) due to the greater availability of free ambient cooling at night. In a very hot climate like Phoenix, the summers are so hot that even the nighttime temperatures are usually too warm to be usefully exploited for free cooling. Similar arguments apply in reverse for the heating season, so the impact of thermal switches is greater when the winters are not too cold (e.g., Phoenix) due to greater availability of free ambient heating in the daytime.

In conclusion, we have developed a voltage-controlled thermal switch with several key features optimized for potential application in building envelopes to reduce the energy required for building heating and cooling. Crucially, the thermal switch is non-volatile and stable in both its on and off states. This means the switch consumes no electricity to hold either steady state for ~99.99% of each day, requiring only brief application of electrical energy during ~0.01% of the day while actively switching between its two stable states. The switch ratio exceeds 10, and the off-state thermal conductivity of $k_{eff,off}$ = 0.045 W $m^{-1}K^{-1}$ is comparable to standard fiberglass batts, which are widely used for static building insulation. This device also shows good cyclability over 1,000 cycles and low energy cost for switching. Based on these measured thermal switch performance values, simulations using realistic wall structures and climate zone data indicate that heating/cooling energy savings in the range 10%–70% depending on the climate zone can be achieved when combining these thermal switches with a thin layer of PCM.

The presented thermal switch demonstrates a simple and efficient approach to realize "dynamic insulation."[14–18,31] In principle, its application and benefits are not limited by climate type but rather are shown by simulation to offer benefits for both heating- and cooling-season-dominated climate zones, though the greatest benefits are realized only when the daily exterior temperatures cross significantly both above and below the desired interior temperature within a 24 h period. This study highlights the benefits of actively controlling the thermal properties of the building envelope for building energy management.

EXPERIMENTAL PROCEDURES

Resource availability

Lead contact

Further information and requests for resources and materials should be directed to and will be fulfilled by the lead contact, Chris Dames (cdames@berkeley.edu).

Materials availability

This study did not generate new unique materials.

Data and code availability

All data needed to support the findings of this study are available from the lead contact upon reasonable request.

Experimental methods

The thermal switch device frame was constructed with 6061 Al alloy and HDPE plastic. The SMA wires are commercial 0.25 mm diameter Flexinol Ni/Ti alloy wires with transition temperature 70°C. The TIM is H48-2K from t-Global Technology, with thermal conductivity 2.3 W $m^{-1}K^{-1}$ and thickness 0.1 mm according to the vendor. The film heater is KHA-404/5 from OMEGA with 10 × 10 cm size and maximum 80 W power. K-type thermocouples from OMEGA (diameter = 0.036 mm) were used to measure temperature. Silicone grease was used to reduce thermal contact resistance between thermocouples and device. Temperature data were taken by a Keithley 2700 data acquisition system.

SUPPLEMENTAL INFORMATION

Supplemental information can be found online at https://doi.org/10.1016/j.xcrp.2022.100960.

ACKNOWLEDGMENTS

The authors gratefully acknowledge funding support by the Building Technologies Program in the Office of Energy Efficiency and Renewable Energy of the US Department of Energy under contract nos. DEAC02-05CH11231 and DE-AC36-08GO28308. The views expressed in the article do not necessarily represent the views of the DOE or the US government. The US government retains, and the publisher, by accepting the article for publication, acknowledges that the US government retains, a nonexclusive, paid-up, irrevocable, worldwide license to publish or reproduce the published form of this work, or allow others to do so, for US government purposes. R.K. thanks Chuck Booten, Judith Vidal, and Roderick Jackson for their guidance and support.

AUTHOR CONTRIBUTIONS

C.D., S.K., and R.P. conceived the idea of using a thermal switch in buildings in this way. C.D. and R.M. conceived and designed the study, with feedback from R.P. and S.K. R.M. designed and performed the experiments. R.K. designed and conducted the simulations of energy savings considering climate zones. R.M. wrote the paper with input from R.K and C.D. All authors discussed the results and commented on the manuscript.

DECLARATION OF INTERESTS

The authors declare no competing interests.

Received: April 1, 2022
Revised: May 31, 2022
Accepted: June 8, 2022
Published: July 7, 2022

REFERENCES

1. 2019 Global Status Report for Buildings and Construction (International Energy Agency). https://www.unep.org/resources/publication/2019-global-status-report-buildings-and-construction-sector.
2. Urge-Vorsatz, D., Cabeza, L.F., Serrano, S., Barreneche, C., and Petrichenko, K. (2015). Heating and cooling energy trends and drivers in buildings. Renew. Sustain. Energy Rev. *41*, 85–98. https://doi.org/10.1016/j.rser.2014.08.039.
3. Urge-Vorsatz, D., Petrichenko, K., Staniec, M., and Eom, J. (2013). Energy use in buildings in a long-term perspective. Curr. Opin. Environ. Sustain. *5*, 141–151. https://doi.org/10.1016/j.cosust.2013.05.004.
4. 2021 April EIA Monthly Review (US Energy Information Administration). https://www.eia.gov/totalenergy/data/monthly/archive/00352104.pdf.
5. Use of Energy Explained: Energy Use in Homes (US Energy Information Administration). https://www.eia.gov/energyexplained/use-of-energy/homes.php.
6. Booten, C., Rao, P., Rapp, V., Jackson, R., and Prasher, R. (2021). Theoretical minimum thermal load in buildings. Joule *5*, 24–46. https://doi.org/10.1016/j.joule.2020.12.015.
7. Zhao, B., Wang, C.Y., Hu, M.K., Ao, X.Z., Liu, J., Xuan, Q.D., and Pei, G. (2022). Light and thermal management of the semi-transparent radiative cooling glass for buildings. Energy *238*, 121761. https://doi.org/10.1016/j.energy.2021.121761.
8. Wong, K.V., and Chan, R. (2014). Smart glass and its potential in energy savings. J. Energy Resour. Technol. *136*, 012002. https://doi.org/10.1115/1.4024768.
9. Alias, A., Abhijith, R., and Thankachan, V. (2018). Review on applications of smart glass in green buildin. In Green Buildings and Sustainable Engineering -Proceedings of GBSE 2018, H. Drück, R.G. Pillai, M.G. Tharian, and A.Z. Majeed, eds. (Springer).
10. Tang, K., Dong, K., Li, J., Gordon, M.P., Reichertz, F.G., Kim, H., Rho, Y., Wang, Q., Lin, C.-Y., Grigoropoulos, C.P., et al. (2021). Temperature-adaptive radiative coating for all-season household thermal regulation. Science *374*, 1504–1509. https://doi.org/10.1126/science.abf7136.
11. Rawat, M., and Singh, R.N. (2021). A study on the comparative review of cool roof thermal performance in various regions. Energy Built Environ. *3*, 327–347.
12. Al-Obaidi, K.M., Ismail, M., and Abdul Rahman, A.M. (2014). Passive cooling techniques through reflective and radiative roofs in tropical houses in Southeast Asia: a literature review. Front. Archit. Res *3*, 283–297. https://doi.org/10.1016/j.foar.2014.06.002.
13. Winiarski, D., Halverson, M., and Jiang, W. (2007). Analysis of Building Envelope Construction in 2003 CBECS (Pacific Northwest National Laboratory (PNNL)).
14. Menyhart, K., and Krarti, M. (2017). Potential energy savings from deployment of Dynamic Insulation Materials for US residential buildings. Build. Environ. *114*, 203–218. https://doi.org/10.1016/j.buildenv.2016.12.009.
15. Sadineni, S.B., Madala, S., and Boehm, R.F. (2011). Passive building energy savings: a review of building envelope components. Renew. Sustain. Energy Rev. *15*, 3617–3631. https://doi.org/10.1016/j.rser.2011.07.014.
16. Clark, W.W., Schaefer, L.A., Knotts, W.A., Mo, C., and Kimber, M. (2013) Variable thermal insulation. USA patent US 20130081786A1, patent application US 20130081786A1.
17. Park, B., Srubar, W.V., and Krarti, M. (2015). Energy performance analysis of variable thermal resistance envelopes in residential buildings. Energy Build. *103*, 317–325. https://doi.org/10.1016/j.enbuild.2015.06.061.
18. Jelle, B.P., Gustavsen, A., and Baetens, R. (2010). The path to the high performance thermal building insulation materials and solutions of tomorrow. J. Build. Phys. *34*, 99–123. https://doi.org/10.1177/1744259110372782.
19. Kishore, R.A., Bianchi, M.V.A., Booten, C., Vidal, J., and Jackson, R. (2021). Enhancing building energy performance by effectively using phase change material and dynamic insulation in walls. Appl. Energy *283*, 116306. https://doi.org/10.1016/j.apenergy.2020.116306.
20. Henry, A., Prasher, R., and Majumdar, A. (2020). Five thermal energy grand challenges for decarbonization. Nat. Energy *5*, 635–637. https://doi.org/10.1038/s41560-020-0675-9.
21. Wehmeyer, G., Yabuki, T., Monachon, C., Wu, J.Q., and Dames, C. (2017). Thermal diodes, regulators, and switches: physical mechanisms and potential applications. Appl. Phys. Rev. *4*, 041304. https://doi.org/10.1063/1.5001072.
22. Jelle, B.P. (2011). Traditional, state-of-the-art and future thermal building insulation materials and solutions - properties, requirements and possibilities. Energy Build. *43*, 2549–2563. https://doi.org/10.1016/j.enbuild.2011.05.015.
23. Taylor, B.J., Cawthorne, D.A., and Imbabi, M.S. (1996). Analytical investigation of the steady-state behaviour of dynamic and diffusive building envelopes. Build. Environ. *31*, 519–525. https://doi.org/10.1016/0360-1323(96)00022-4.
24. Kosny, J., Kossecka, E., Brzezinski, A., Tleoubaev, A., and Yarbrough, D. (2012). Dynamic thermal performance analysis of fiber insulations containing bio-based phase change materials (PCMs). Energy Build. *52*, 122–131. https://doi.org/10.1016/j.enbuild.2012.05.021.
25. Bueno, B., Norford, L., Pigeon, G., and Britter, R. (2012). A resistance-capacitance network model for the analysis of the interactions between the energy performance of buildings and the urban climate. Build. Environ. *54*, 116–125. https://doi.org/10.1016/j.buildenv.2012.01.023.
26. Mumme, S., James, N., Salonvaara, M., Shrestha, S., and Hun, D.N. (2020). Smart and efficient building envelopes: thermal switches and thermal storage for energy savings and load flexibility. Ashrae Trans. *126*, 140–148.
27. Sun, Y.J., Wang, S.W., Xiao, F., and Gao, D.C. (2013). Peak load shifting control using different cold thermal energy storage facilities in commercial buildings: a review. Energy Convers. Manag. *71*, 101–114. https://doi.org/10.1016/j.enconman.2013.03.026.
28. Duffin, R.J., and Knowles, G. (1981). Temperature control of buildings by adobe wall design. Sol. Energy *27*, 241–249. https://doi.org/10.1016/0038-092x(81)90125-0.
29. Sadineni, S.B., and Boehm, R.F. (2012). Measurements and simulations for peak electrical load reduction in cooling dominated climate. Energy *37*, 689–697. https://doi.org/10.1016/j.energy.2011.10.026.
30. Kishore, R.A., Bianchi, M.V.A., Booten, C., Vidal, J., and Jackson, R. (2020). Optimizing PCM-integrated walls for potential energy savings in US Buildings. Energy Build. *226*, 110355. https://doi.org/10.1016/j.enbuild.2020.110355.
31. Cui, H.X., and Overend, M. (2019). A review of heat transfer characteristics of switchable insulation technologies for thermally adaptive building envelopes. Energy Build. *199*, 427–444. https://doi.org/10.1016/j.enbuild.2019.07.004.
32. Ciampi, M., Leccese, F., and Tuoni, G. (2003). Ventilated facades energy performance in summer cooling of buildings. Sol. Energy *75*, 491–502. https://doi.org/10.1016/j.solener.2003.09.010.
33. Tso, C.Y., and Chao, C.Y.H. (2016). Solid-state thermal diode with shape memory alloys. Int. J. Heat Mass Tran. *93*, 605–611. https://doi.org/10.1016/j.ijheatmasstransfer.2015.10.045.
34. Hao, M.L., Li, J., Park, S., Moura, S., and Dames, C. (2018). Efficient thermal management of Li-ion batteries with a passive interfacial thermal regulator based on a shape memory alloy. Nat. Energy *3*, 899–906. https://doi.org/10.1038/s41560-018-0243-8.
35. Benafan, O., Notardonato, W.U., Meneghelli, B.J., and Vaidyanathan, R. (2013). Design and development of a shape memory alloy activated heat pipe-based thermal switch. Smart Mater. Struct. *22*, 105017. https://doi.org/10.1088/0964-1726/22/10/105017.
36. El-Genk, M.S.; United States. Department of Energy; United States. National Aeronautics and Space Administration; American Astronautical Society; University of New Mexico. Institute for Space and Nuclear Power Studies; American Institute of Physics (2002). Space Technology and Applications International Forum–STAIF 2002 (American Institute of Physics).
37. Copic, D., and Hart, A.J. (2015). Corrugated paraffin nanocomposite films as large stroke thermal actuators and self-activating thermal interfaces. ACS Appl Mater Inter *7*, 8218–8224. https://doi.org/10.1021/acsami.5b01141.

38. Gilmore, D.G. (2002). Spacecraft Thermal Control Handbook, Second Edition (Aerospace Press).

39. Wong, M.Y., Tso, C.Y., Ho, T.C., and Lee, H.H. (2021). A review of state of the art thermal diodes and their potential applications. Int. J. Heat Mass Trans. *164*, 120607. https://doi.org/10.1016/j.ijheatmasstransfer.2020.120607.

40. Paul Motzki, S.S. (2016). Bi-stable SMA actuator. In Actuator 16 - 15th International Conference on New Actuators, pp. 317–320.

41. Mohd Jani, J., Leary, M., Subic, A., and Gibson, M.A. (2014). A review of shape memory alloy research, applications and opportunities. Mater Design *56*, 1078–1113. https://doi.org/10.1016/j.matdes.2013.11.084.

42. Sohn, J.W., Kim, G.W., and Choi, S.B. (2018). A state-of-the-art review on robots and medical devices using smart fluids and shape memory alloys. Appl. Sci. *8*, 1928. https://doi.org/10.3390/app8101928.

43. Berardi, U. (2017). The impact of temperature dependency of the building insulation thermal conductivity in the Canadian climate. Energy Proc. *132*, 237–242. https://doi.org/10.1016/j.egypro.2017.09.684.

44. Abdou, A.A., and Budaiwi, I.M. (2005). Comparison of thermal conductivity measurements of building insulation materials under various operating temperatures. J. Build. Phys. *29*, 171–184. https://doi.org/10.1177/1744259105056291.

45. 2015 RECS Square Footage Methodology (U.S. Energy Information Administration). https://www.eia.gov/consumption/residential/reports/2015/squarefootage/pdf/2015_recs_squarefootage.pdf.

46. 2021 Producer Price Index Detailed Reports (U.S. Bureau of Labor Statistics). https://www.bls.gov/ppi/detailed-report/#2021.

47. Shrestha, S.S., Childs, K.W., and Stannard, E.E. (2012). Field Study and Energy-Plus Benchmarks for Energy Saver Homes Having Different Envelope Designs. held in United States.

48. Burleyson, C. (2020). 2012 IECC Climate Zones (R. Pacific Northwest National Laboratory (PNNL)).